Front. Optoelectron. 2020, 13(3): 282–290
https://doi.org/10.1007/s12200-020-1046-7

RESEARCH ARTICLE

Composition engineering to obtain efficient hybrid perovskite light-emitting diodes

Chuanzhong YAN*, Kebin LIN*, Jianxun LU, Zhanhua WEI (✉)

Institute of Luminescent Materials and Information Displays, College of Materials Science and Engineering, Huaqiao University, Xiamen 361021, China

Abstract Metal halide perovskites have received considerable attention in the field of electroluminescence, and the external quantum efficiency of perovskite light-emitting diodes has exceeded 20%. $CH_3NH_3PbBr_3$ has been intensely investigated as an emitting layer in perovskite light-emitting diodes. However, perovskite films comprising $CH_3NH_3PbBr_3$ often exhibit low surface coverage and poor crystallinity, leading to high current leakage, severe nonradiative recombination, and limited device performance. Herein, we demonstrate a rationale for composition engineering to obtain high-quality perovskite films. We first reduce pinholes by adding excess CH_3NH_3Br to the actual $CH_3NH_3PbBr_3$ films, and we then add CsBr to improve the crystalline quality and to passivate nonradiative defects. As a result, the $(CH_3NH_3)_{1-x}Cs_xPbBr_3$ based perovskite light-emitting diodes exhibit significantly improved external quantum and power efficiencies of 6.97% and 25.18 lm/W, respectively, representing an improvement in performance dozens of times greater than that of pristine $CH_3NH_3PbBr_3$-based perovskite light-emitting diodes. Our study demonstrates that composition engineering is an effective strategy for enhancing the device performance of perovskite light-emitting diodes.

Keywords perovskite, light-emitting diode (LED), composition engineering, ion doping

1 Introduction

Recently, metal halide perovskite materials have received considerable attention in the field of light-emitting diodes (LEDs). Perovskite materials have unique advantages, such as high photoluminescence quantum yields (PLQYs), excellent color purity, high defect tolerance, tunable bandgap, wide color gamut, and low cost [1–6]. The first room-temperature operative perovskite light-emitting diodes (Pero-LEDs) were reported by Friend et al. in 2014 [1]. They used three-dimensional (3D) perovskite materials of $MAPbI_{3-x}Cl_x$ ($MA:CH_3NH_3^+$) and $MAPbBr_3$ as the light-emitting layer to prepare near-infrared and green LED devices, the corresponding external quantum efficiencies (EQEs) of which were 0.76% and 0.1%, respectively [1]. To date, tremendous research progress has been accomplished in the fabrication of multicolor-emitting Pero-LEDs and improving their performance [7–14]. In particular, the EQE values of green [15], visible red [16], and near-infrared [17–19] region Pero-LEDs have drastically increased to over 20%. Pero-LEDs have exhibited promising application prospects in the fields of flat displays and solid lighting [20,21].

The chemical formula of metal halide perovskite is generally of the form ABX_3, where A is a monovalent cation (such as MA^+, FA^+:$CH(NH_2)_2^+$, or Cs^+), B is a divalent metal cation (such as Pb^{2+}, Sn^{2+}, or Cu^{2+}), and X is a halogen (such as I^-, Br^-, or Cl^-) or a halogen-like molecule (SCN^-) [22,23]. Among the various perovskite components, $MAPbBr_3$ has great potential for preparing high-efficiency Pero-LEDs. However, it is reported that the most primitive perovskite films comprising $MAPbBr_3$ (i.e., $PbBr_2$:MABr = 1:1) exhibit low surface coverage, poor structural stability, and poor crystalline quality with too many nonradiative defects [24,25]. To improve the film quality of $MAPbBr_3$ perovskite, Lee et al. precisely adjusted the molar proportion of MABr and $PbBr_2$ [4]. They found that a slight excess of MABr can effectively suppress the quenching of excitons caused by the defects of metallic lead (Pb^0). Moreover, they further improved the crystalline quality, reduced the grain size of perovskite

Received May 18, 2020; accepted June 30, 2020

E-mail: weizhanhua@hqu.edu.cn

*These authors contributed equally to this work.

through solvent engineering, and finally boosted the EQE to 8.53% for green Pero-LEDs [4]. In addition, Jin et al. mixed Cs and MA cations to prepare high-quality $Cs_{0.4}MA_{0.6}PbBr_3$ thin films. The as-prepared films exhibited excellent emission properties, and the corresponding Pero-LEDs showed a maximum EQE of ~2.0% [26]. Recently, You et al. found that different organic cations (MA and FA) have a significant impact on the quantum-well structures [27]. $PEA_2(FAPbBr_3)_{n-1}PbBr_4$-based Pero-LEDs showed an impressively higher EQE (15.4%) than that of the $PEA_2(MAPbBr_3)_{n-1}PbBr_4$-based Pero-LEDs devices (0.93%). It was found that there is a PEA_2PbBr_4 phase presented in the $PEA_2(MAPbBr_3)_{n-1}PbBr_4$ film and the insulating nature of the PEA_2PbBr_4 lead to poor hole-injection efficiency and lower carrier mobility [27]. Thus, it can be concluded that the A-side cations have a significant influence on the structure, morphology, and optical properties of perovskite films. Although some progress has been accomplished, there is still much room to further improve the performance of $MAPbBr_3$-based Pero-LEDs through component control strategies.

In this study, we are committed to improving the device performance of the $MAPbBr_3$-based Pero-LED devices through composition engineering. First, we regulate the content of MABr to prepare a nonstoichiometric $MAPbBr_3$ film, and the MABr additive effectively reduces the nonradiative defects (such as vacancies and Pb defects) and increased the surface coverage of perovskite film. Furthermore, we improve the as-prepared $MAPbBr_3$ film quality by doping with CsBr, improving the crystallinity. Nonstoichiometric bromine compound additives (e.g., MABr, CsBr) added to the perovskite precursor have the above-mentioned effects, which could be attributed to the following reasons: 1) The strong bond formed between the bromine and lead atoms eliminates the metallic lead (Pb^0) exposed on the surface of the films. 2) The partial ion (Br^- and MA^+) concentration increases. These ions have a higher concentration in the precursor and the opportunity to passivate the inherent vacancy defects of films. 3) A modification in the crystallization behavior is observed. Bromine compound additives increase the partial ion concentration in the precursor; thus, the supersaturation concentration is reached faster during the process of spin coating. These changes promote the generation of a large number of crystal nuclei that grow in an island-like manner and form a thin film with full coverage and high crystallinity. As a result, we have obtained a high-quality $MA_{1-x}Cs_xPbBr_3$ perovskite emitter with a pinhole-free surface and suppressed defects. The optimized Pero-LEDs devices exhibit peak EQE and power efficiency (PE) values of 6.97% and 25.18 lm/W, respectively. These results represent an improvement in performance dozens of times that of pristine $MAPbBr_3$ Pero-LEDs devices.

2 Experimental section

2.1 Materials

Unless otherwise stated, all chemicals were purchased from Sigma-Aldrich (America) and used as received.

2.2 Perovskite precursor preparation

The $MAPbBr_3$ perovskite precursor was obtained by dissolving 0.1120 g of MABr (1 mmol, Dyesol, Australia 99.99%) powder and 0.3670 g of $PbBr_2$ (1 mmol, 99.99%) powder in 2 mL of dimethyl sulfoxide (DMSO, 98%). The nonstoichiometric $MAPbBr_3$ perovskite precursor was prepared using the same procedure with the molar ratio of $PbBr_2$:MABr = 1:1.1 to 1:1.3. The $PbBr_2$:MABr = 1:1.1 sample was denoted as $MAPbBr_3$-excess. The precursor of $MAPbBr_3$-excess:(X)CsBr (99.999%) was obtained by adding excess CsBr (X = 0.4, 0.8, and 1.2 mmol) to the as-prepared $MAPbBr_3$-excess precursor. Moreover, the mixed solution was stirred for 12 h at room temperature, remained static for another 24 h prior to its use, and the supernatant was used to prepare the perovskite films.

2.3 Device fabrication

Prepatterned indium tin oxide (ITO) glass substrates (AGC, Japan, 7 Ω, 20 mm × 20 mm) were sequentially ultrasonicated in detergent water, deionized water, acetone, isopropanol, and ethanol for 20 min, respectively. Then, the ITO substrates were dried with compressed nitrogen gas and were further treated using a UV ozone cleaner for 30 min. Poly (3,4-ethylene dioxythiophene) polystyrene sulfonate (PEDOT:PSS, Clevious-AI4083, Germany) was spin-coated on the as-cleaned ITO substrates at 4000 r/min for 50 s, and the substrates were baked at 130°C for 15 min. Then, the substrates were transferred into an N_2-filled glove box. A 30-μL perovskite precursor solution was spin-coated on the substrates at 2000 r/min for 60 s, and 500 μL of toluene was quickly dropped onto the surface as an antisolvent at 35 s. Subsequently, polymethyl methacrylate (PMMA, TCI Tokyo, Japan, 99.99%) dissolved in acetone solvent, and 60 μL of PMMA solution (0.4 mg/mL) was dropped onto the perovskite film through the same spin-coating procedure. For the next steps, the as-prepared substrates were transferred into a thermal evaporator. Then, 50 nm of 4,6-bis(3,5-di(pyridin-3-yl) phenyl)-2-methylpyrimidine (B3PYMPM, Lumtec Taiwan, China, 99.99%), 1.5 nm of LiF (98%), and 90 nm of Al were sequentially deposited at a chamber vacuum pressure of 5.0×10^{-4} Pa. The deposition rates of B3PYMPM, LiF, and Al were 1.5, 0.1, and 2 Å/s, respectively. The Pero-LED device's active area was determined by the overlap area between the ITO and Al electrodes, and it was 3 mm^2.

2.4 Characterization

Field-emission scanning electron microscope (SEM) (Hitachi S-8000, Japan) was employed to characterize the surface morphology. X-ray diffraction (XRD) patterns were measured using a Smartlab X-ray diffractometer (Rigaku, Japan). Steady-state photoluminescence (PL) spectra, absorbance spectra, and electroluminescence characteristics were recorded using a QE-Pro65 (Ocean Optics, America) in an N_2-filled glovebox. All electroluminescence measurements of Pero-LEDs were collected in the glovebox filled with N_2. The current density–voltage (*J–V*) curves of the device were obtained using a Keithley 2400 instrument, and the luminance was simultaneously measured using a luminance meter (Konica Minolta, Japan, CS200). The applied bias voltage varied from 0 to 7 V and the scan rate was 0.2 V/s. The current efficiency was obtained by dividing the luminance by the current density. The EQE was calculated using Lambertian emission profiles and the obtained electroluminescence spectra.

3 Results and discussion

It is widely reported that $MAPbBr_3$ films comprising $PbBr_2$:MABr = 1:1.0 always exhibit poor surface coverage and low PLQYs. This is mostly attributed to the existence of a large number of Br vacancies, which serve as nonradiative recombination centers [28,29]. Small amounts of MABr additive could increase the content of Br^- and reduce Br vacancies, whereas large amounts of additives will induce the formation of other impurity phases. We attempted to eliminate the Br vacancies by adding excess MABr to the $MAPbBr_3$. We tuned the molar ratio of $PbBr_2$:MABr from 1:1.0 to 1:1.3, and the corresponding histograms of peak current efficiency (CE) data are shown in Fig. 1(a). A remarkable CE enhancement in $MAPbBr_3$ with excess MABr is observed, which is optimized at the molar ratio of $PbBr_2$:MABr = 1:1.1 (denoted as $MAPbBr_3$-excess hereafter). Figure 1(b) shows the steady-state PL spectra of the corresponding perovskite films, and the inset is an image of the perovskite films under UV illumination (365 nm). The $MAPbBr_3$-excess film shows a much higher PL intensity than that of the $MAPbBr_3$ film, indicating reduced Br vacancies in the $MAPbBr_3$-excess film. We further compared the surface morphology of the films through SEM. As shown in Fig. 1 (c), the $MAPbBr_3$ film exhibits poor surface morphology with high density of pinholes. On the contrary, as shown in Fig. 1(d), the $MAPbBr_3$-excess film exhibits a uniform surface with fewer pinholes, where the excess MABr additive increases the concentration of MA^+ and Br^- ions and promotes generation of crystal nuclei to form a high-quality perovskite film. Figure 1(e) presents the corresponding XRD patterns, in which the diffraction peaks of $MAPbBr_3$ film and $MAPbBr_3$-excess film are nearly the same, indicating that excess MABr does not change the crystal structure. After preliminary optimization of the composition of the perovskite, we prepared Pero-LEDs devices to evaluate the device performance. Figure 1(f) shows the typical current density–luminance–voltage (*J–L–V*) curves of the Pero-LEDs based on these two perovskites, from which we see that the luminance of the $MAPbBr_3$-excess device is significantly higher than that of the $MAPbBr_3$ device. In particular, when the applied voltage exceeds approximately 6.5 V, the $MAPbBr_3$ device with poor film quality deteriorates, leading to a decrease in current density. On the contrary, the $MAPbBr_3$-excess device with fewer defects degrades more gradually and the current density continues increasing to 7.0 V. The maximum CE of the $MAPbBr_3$ and $MAPbBr_3$-excess devices are 0.149 and 2.46 cd/A, respectively. These results indicate that an excess of MABr can reduce the intrinsic defects and pinholes of $MAPbBr_3$ films, enhancing the device performance of Pero-LEDs.

As proposed, we further doped the perovskite with Cs^+ ions by adding CsBr to the $MAPbBr_3$-excess perovskite precursor to effectively regulate the grain size and further eliminate nonradiative defects. A schematic diagram of the crystal structure with Cs^+ ion doping is shown in Fig. 2(a), where Cs^+ ions partially replace MA^+ ions to form an ion-doped perovskite of $MA_{1-x}Cs_xPbBr_3$. The PL spectra (Fig. 2(b)) show that doping with CsBr can significantly improve the fluorescence intensity of the perovskite films and that the doping ratio has a significant influence on the PL intensity of the perovskite films. In particular, the $MAPbBr_3$-excess:CsBr = 1:0.8 exhibits the highest PL intensity. Figure 2(c) shows the $(\alpha h\nu)^2$-photon energy (eV) curves of different mixed perovskites based on the calculation of Tauc plot, where the films were deposited on the as-prepared PEDOT:PSS/ITO substrates. With the increase in the molar ratio of CsBr from 0 to 1.2, the absorption band edge is increasingly blue-shifted, and the corresponding optical band gap increases from ~2.33 to ~2.49 eV, corresponding to a PL peak center blue-shift from 538 to 505 nm (Fig. 2(b)). This is mainly due to the Pb-Br_6 octahedra tilting after the partial substitution of smaller Cs^+ cations [30]. The XRD patterns of $MAPbBr_3$-excess with different proportions of CsBr and a standard phase of $CsPbBr_3$ (PDF#54-0752) were collected and are shown in Fig. 2(d). The perovskite films exhibit a monophase of $MA_{1-x}Cs_xPbBr_3$, and no $CsPbBr_3$ phase can be observed. The $MAPbBr_3$-excess films exhibit two main peaks at 14.78° and 29.98°, corresponding to the (100) and (200) planes, respectively. The partially magnified diffraction peaks (Fig. 2(e)) show that both peaks shift toward a higher diffraction angle with an increased Cs^+ cation molar ratio. This shift could be attributed to the smaller Cs^+ (1.81 Å) ions partially

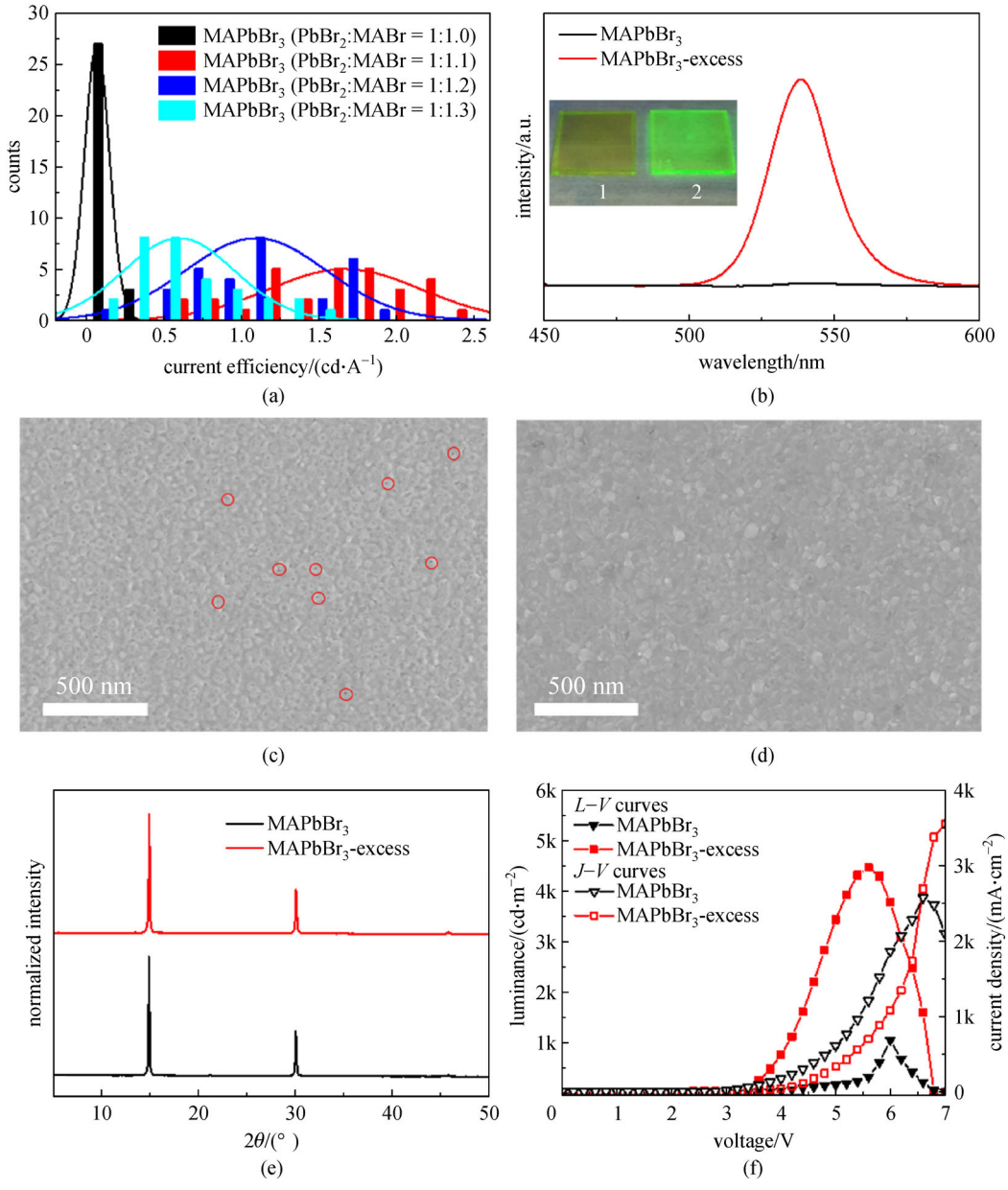

Fig. 1 MABr additive enhances the perovskite film quality and the corresponding device performance. (a) Distribution of CE of the Pero-LEDs. (b) PL spectra of the perovskite films with inset of an image of perovskite films (1: $MAPbBr_3$, 2: $MAPbBr_3$-excess) under UV illumination (365 nm). SEM images of (c) $MAPbBr_3$ and (d) $MAPbBr_3$-excess perovskite films (pinholes are indicated by red circles). (e) XRD patterns of the perovskite films. (f) Current density–luminance–voltage (*L*–*J*–*V*) curves of the best-performing Pero-LEDs

substituting the larger MA^+ (2.18 Å) ions in the perovskite crystal structure, reducing the interplanar crystal spacing.

To investigate the impact of Cs^+ doping on the grain size and surface morphology of perovskite films, the surface morphologies of the four typical perovskite films were characterized using top-view SEM. As shown in Figs. 3(a)–3(c), it can be seen that the grain size gradually increased with the doping concentration of Cs^+ ions from 0 to 0.8. The additional CsBr might reduce the stripping ability of toluene, resulting in a slower nucleation rate of perovskite and reducing the number of nucleation sites, thereby increasing the size of perovskite grains. In this regard, many previous works have shown that there are few radiation-free recombination defects inside large-grained perovskite crystals, and large grains might be beneficial for the charge transport [31,32]. However, when we further increased the doping concentration of CsBr to 1.2, we found that the grain boundaries were significantly increased, and the film coverage was significantly decreased (Fig. 3(d)).

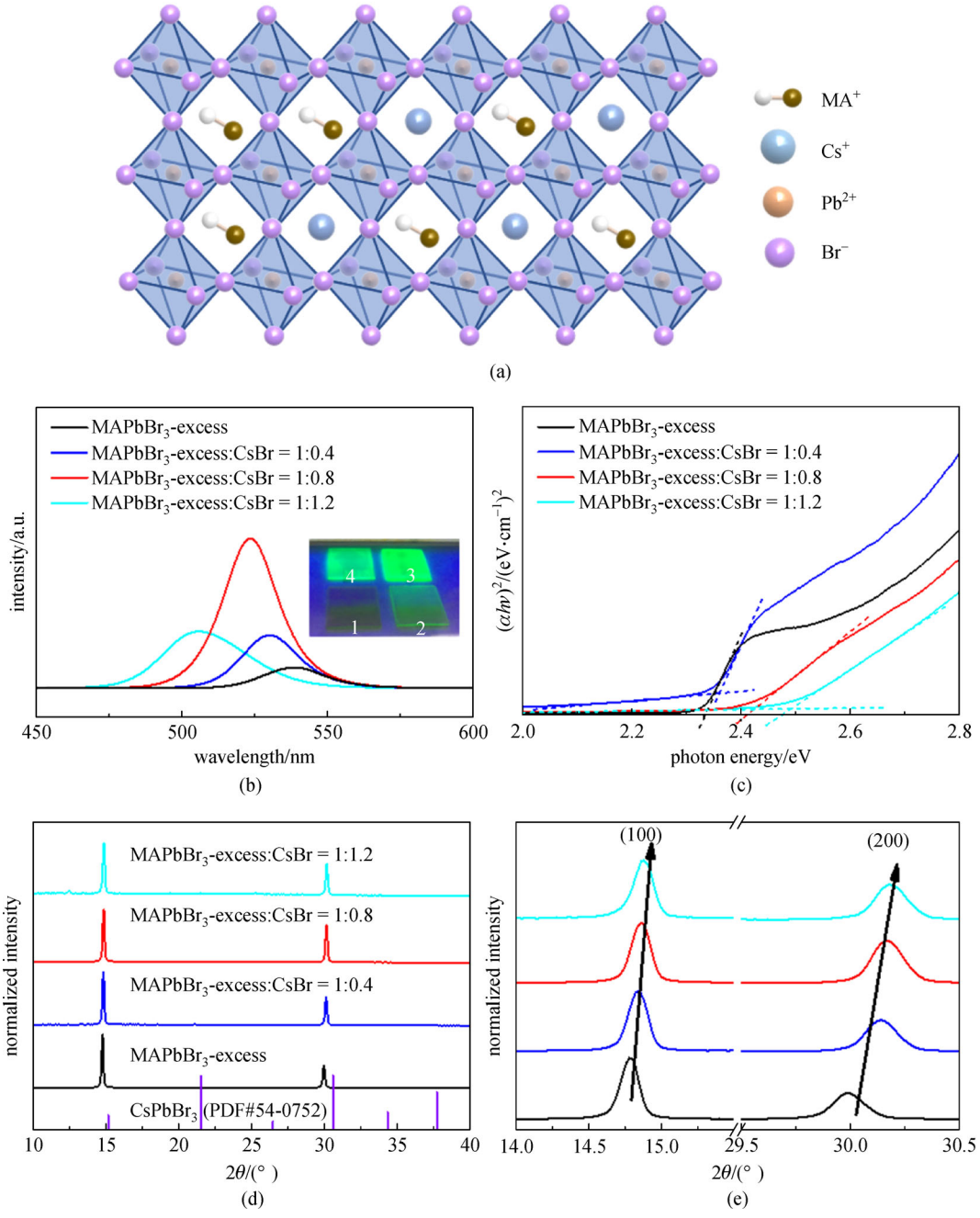

Fig. 2 CsBr doping improves the film quality. (a) Schematic of crystal structure of the $MAPbBr_3$ doped with CsBr. (b) PL spectra of the perovskite films, inset is an image of perovskite films (1: $MAPbBr_3$-excess, 2: $MAPbBr_3$-excess:CsBr = 1:0.4, 3: $MAPbBr_3$-excess:CsBr = 1:0.8, 4: $MAPbBr_3$-excess:CsBr = 1:1.2) under UV illumination (365 nm). (c) $(\alpha h\nu)^2$-photon energy (eV) curve of the perovskite films. (d) XRD patterns of the perovskite films. (e) Partially magnified XRD patterns showing (100) and (200) peaks

In general, the perovskite film prepared with the component of $MAPbBr_3$-excess:CsBr = 1:0.8 showed much better emission properties and a more uniform surface with larger grain size, which might be beneficial to carrier transport and suppression of nonradiative recombination in Pero-LEDs.

To evaluate the electroluminescence (EL) properties of the typical perovskite films, we fabricated Pero-LEDs devices with a multilayered architecture of ITO/PEDOT:PSS/Perovskite/PMMA/B3PYMPM/LiF/Al. The PEDOT:PSS and B3PYMPM served as the hole transfer layer and electron transport layer, respectively. Moreover, the PMMA served as an electron blocking layer, the LiF served as an electron-injection layer, and the Al served as

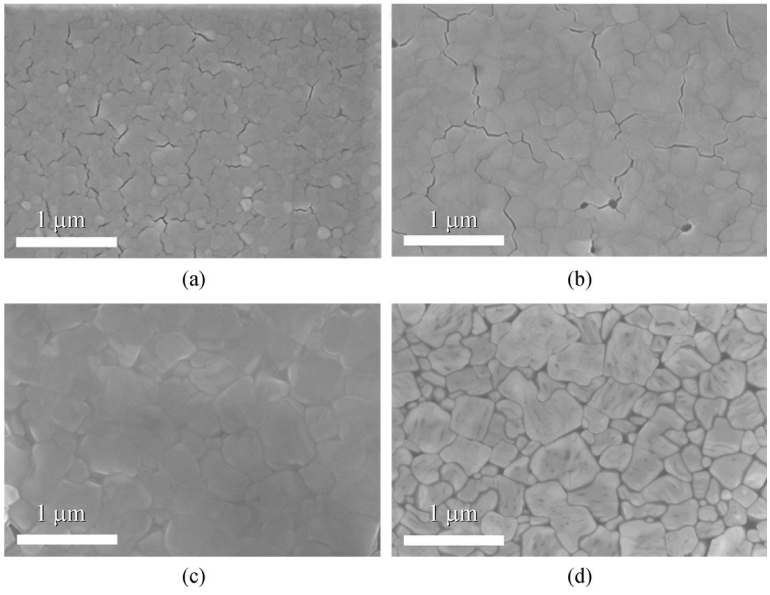

Fig. 3 SEM images of perovskite films. (a) $MAPbBr_3$-excess. (b) $MAPbBr_3$-excess:CsBr = 1:0.4. (c) $MAPbBr_3$-excess:CsBr = 1:0.8. (d) $MAPbBr_3$-excess:CsBr = 1:1.2 (Apparent cracks in images are caused by the electron-beam irradiation during SEM)

the cathode. The corresponding schematic diagram and energy band diagram of the Pero-LEDs are shown in Figs. 4(a) and 4(b), respectively. The *J–V* curves and *L–V* curves for the Pero-LEDs fabricated with different perovskite mixtures are shown in Figs. 4(c) and 4(d), and the detailed EL parameters are summarized in Table 1. It can be seen that an appropriate CsBr doping ratio can not only effectively reduce the leakage current but also increase the luminance of Pero-LEDs devices. The best-performing Pero-LEDs with $MAPbBr_3$-excess:CsBr = 1:0.8 exhibit higher luminance (15059 cd/m^2) and lower turn-on voltage (V_{on}, ~2.4 V) than the other devices, showing a maximum EQE of 6.97%. To evaluate the device reproducibility, we prepared 20 Pero-LEDs devices for each perovskite doping concentration under the same preparation conditions, and CE distribution is shown in Fig. 4(e). We can see that the Cs^+ ion doping has a significant influence on the device performance and that the Pero-LEDs based on $MAPbBr_3$-excess:CsBr = 1:0.8 exhibit the best device performance with an average CE value of 21.11 cd/A. Moreover, as shown in Fig. 4(f), the corresponding Pero-LEDs presents a stable EL emission peak at 525 nm, corresponding to the Commission Internationale de ÍEclairage (CIE) color coordinate of (0.21, 0.60).

4 Conclusions

In summary, we have obtained high-quality $MA_{1-x}Cs_xPbBr_3$ perovskite films through a step-by-step perovskite composition modulation, i.e., adding MABr additive and doping with CsBr. The as-prepared $MA_{1-x}Cs_xPbBr_3$ perovskite films exhibit strong PL intensity and fewer pinholes, which is suitable for the fabrication of highly efficient Pero-LEDs. A higher-quality emitting layer can not only improve carrier recombination but also reduce the leakage current in Pero-LEDs devices. Furthermore, we demonstrate that Pero-LEDs with an emission layer of $MAPbBr_3$-excess:CsBr = 1:0.8 have a maximum EQE of 6.97% and peak PE of 25.18 lm/W. The improvement in the Pero-LEDs performance is owing to high-quality perovskite films suppressing nonradiative recombination loss. Our study provides an effective component control strategy to enhance the performance of perovskite optoelectronic devices.

Table 1 EL parameters of the Pero-LEDs with different molar ratios of $MAPbBr_3$-excess:CsBr

molar ratio of $MAPbBr_3$-excess:CsBr	L_{max}/(cd·m^{-2})	CE_{max}/(cd·A^{-1})	EQE_{max}/%	V_{on}/V	PE_{max}/(lm·W^{-1})
1:0	4452	2.46	0.63	~2.8	2.12
1:0.4	13,450	8.23	2.21	~2.6	6.06
1:0.8	15,059	25.80	6.97	~2.4	25.18
1:1.2	13,720	17.99	4.84	~2.4	14.13

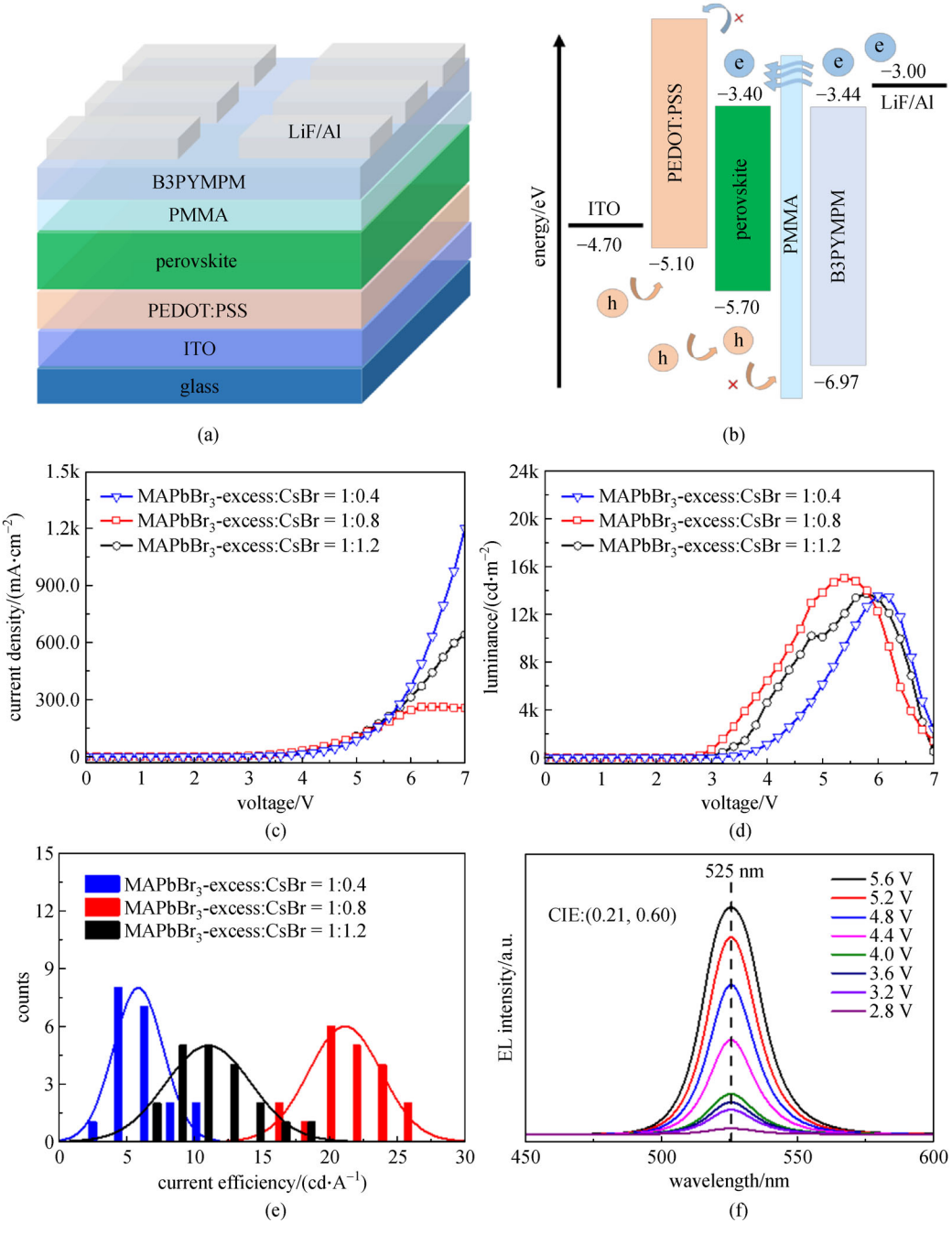

Fig. 4 Fabrication and performance evaluation of Pero-LEDs devices. (a) Schematic diagram of the Pero-LEDs devices. (b) Energy-level diagram of the Pero-LEDs devices. (c) *J*–*V* curves. (d) *L*–*V* curves. (e) Distribution of the CE of the Pero-LEDs fabricated with different perovskites. (f) Electroluminescence spectra at different driving voltages of the Pero-LEDs based on $MAPbBr_3$-excess:CsBr = 1:0.8

Acknowledgements The work was financially supported by the National Natural Science Foundation of China (Grant Nos. 51802102, 21805101, and 51902110), Natural Science Foundation of Fujian Province (No. 2019J01057), Promotion Program for Young and Middle-aged Teacher in Science and Technology Research of Huaqiao University (No. ZQN-PY607), and Scientific Research Funds of Huaqiao University (Nos. 16BS201, 17BS409, and 19BS105).

References

1. Tan Z K, Moghaddam R S, Lai M L, Docampo P, Higler R, Deschler F, Price M, Sadhanala A, Pazos L M, Credgington D, Hanusch F, Bein T, Snaith H J, Friend R H. Bright light-emitting diodes based

on organometal halide perovskite. Nature Nanotechnology, 2014, 9 (9): 687–692

2. Song J, Li J, Li X, Xu L, Dong Y, Zeng H. Quantum dot light-emitting diodes based on inorganic perovskite cesium lead halides ($CsPbX_3$). Advanced Materials, 2015, 27(44): 7162–7167
3. Yuan M, Quan L N, Comin R, Walters G, Sabatini R, Voznyy O, Hoogland S, Zhao Y, Beauregard E M, Kanjanaboos P, Lu Z, Kim D H, Sargent E H. Perovskite energy funnels for efficient light-emitting diodes. Nature Nanotechnology, 2016, 11(10): 872–877
4. Cho H, Jeong S H, Park M H, Kim Y H, Wolf C, Lee C L, Heo J H, Sadhanala A, Myoung N, Yoo S, Im S H, Friend R H, Lee T W. Overcoming the electroluminescence efficiency limitations of perovskite light-emitting diodes. Science, 2015, 350(6265): 1222–1225
5. Wei Z, Perumal A, Su R, Sushant S, Xing J, Zhang Q, Tan S T, Demir H V, Xiong Q. Solution-processed highly bright and durable cesium lead halide perovskite light-emitting diodes. Nanoscale, 2016, 8(42): 18021–18026
6. Wei Z, Xing J. The rise of perovskite light-emitting diodes. Journal of Physical Chemistry Letters, 2019, 10(11): 3035–3042
7. Wang J, Wang N, Jin Y, Si J, Tan Z K, Du H, Cheng L, Dai X, Bai S, He H, Ye Z, Lai M L, Friend R H, Huang W. Interfacial control toward efficient and low-voltage perovskite light-emitting diodes. Advanced Materials, 2015, 27(14): 2311–2316
8. Li G, Rivarola F W R, Davis N J L K, Bai S, Jellicoe T C, de la Peña F, Hou S, Ducati C, Gao F, Friend R H, Greenham N C, Tan Z K. Highly efficient perovskite nanocrystal light-emitting diodes enabled by a universal crosslinking method. Advanced Materials, 2016, 28(18): 3528–3534
9. Wang N, Cheng L, Ge R, Zhang S, Miao Y, Zou W, Yi C, Sun Y, Cao Y, Yang R, Wei Y, Guo Q, Ke Y, Yu M, Jin Y, Liu Y, Ding Q, Di D, Yang L, Xing G, Tian H, Jin C, Gao F, Friend R H, Wang J, Huang W. Perovskite light-emitting diodes based on solution-processed self-organized multiple quantum wells. Nature Photonics, 2016, 10(11): 699–704
10. Xiao Z, Kerner R A, Zhao L, Tran N L, Lee K M, Koh T W, Scholes G D, Rand B P. Efficient perovskite light-emitting diodes featuring nanometre-sized crystallites. Nature Photonics, 2017, 11(2): 108–115
11. Zhang L, Yang X, Jiang Q, Wang P, Yin Z, Zhang X, Tan H, Yang Y M, Wei M, Sutherland B R, Sargent E H, You J. Ultra-bright and highly efficient inorganic based perovskite light-emitting diodes. Nature Communications, 2017, 8(1): 15640
12. Wu Y, Wei C, Li X, Li Y, Qiu S, Shen W, Cai B, Sun Z, Yang D, Deng Z, Zeng H. *In situ* passivation of $PbBr_6^{4-}$ octahedra toward blue luminescent $CsPbBr_3$ nanoplatelets with near 100% absolute quantum yield. ACS Energy Letters, 2018, 3(9): 2030–2037
13. Xing J, Zhao Y, Askerka M, Quan L N, Gong X, Zhao W, Zhao J, Tan H, Long G, Gao L, Yang Z, Voznyy O, Tang J, Lu Z H, Xiong Q, Sargent E H. Color-stable highly luminescent sky-blue perovskite light-emitting diodes. Nature Communications, 2018, 9 (1): 3541
14. Lu J, Feng W, Mei G, Sun J, Yan C, Zhang D, Lin K, Wu D, Wang K, Wei Z. Ultrathin PEDOT:PSS enables colorful and efficient perovskite light-emitting diodes. Advanced Science, 2020, 7(11): 2000689
15. Lin K, Xing J, Quan L N, de Arquer F P G, Gong X, Lu J, Xie L, Zhao W, Zhang D, Yan C, Li W, Liu X, Lu Y, Kirman J, Sargent E H, Xiong Q, Wei Z. Perovskite light-emitting diodes with external quantum efficiency exceeding 20 percent. Nature, 2018, 562(7726): 245–248
16. Chiba T, Hayashi Y, Ebe H, Hoshi K, Sato J, Sato S, Pu Y J, Ohisa S, Kido J. Anion-exchange red perovskite quantum dots with ammonium iodine salts for highly efficient light-emitting devices. Nature Photonics, 2018, 12(11): 681–687
17. Zhao X, Tan Z K. Large-area near-infrared perovskite light-emitting diodes. Nature Photonics, 2020, 14(4): 215–218
18. Cao Y, Wang N, Tian H, Guo J, Wei Y, Chen H, Miao Y, Zou W, Pan K, He Y, Cao H, Ke Y, Xu M, Wang Y, Yang M, Du K, Fu Z, Kong D, Dai D, Jin Y, Li G, Li H, Peng Q, Wang J, Huang W. Perovskite light-emitting diodes based on spontaneously formed submicrometre-scale structures. Nature, 2018, 562(7726): 249–253
19. Xu W, Hu Q, Bai S, Bao C, Miao Y, Yuan Z, Borzda T, Barker A J, Tyukalova E, Hu Z, Kawecki M, Wang H, Yan Z, Liu X, Shi X, Uvdal K, Fahlman M, Zhang W, Duchamp M, Liu J M, Petrozza A, Wang J, Liu L M, Huang W, Gao F. Rational molecular passivation for high-performance perovskite light-emitting diodes. Nature Photonics, 2019, 13(6): 418–424
20. Meredith P, Armin A. LED technology breaks performance barrier. Nature, 2018, 562(7726): 197–198
21. Service R F. Perovskite LEDs begin to shine. Science, 2019, 364 (6444): 918
22. Quan L N, García de Arquer F P, Sabatini R P, Sargent E H. Perovskites for light emission. Advanced Materials, 2018, 30(45): 1801996
23. Xie L, Song P, Shen L, Lu J, Liu K, Lin K, Feng W, Tian C, Wei Z. Revealing the compositional effect on the intrinsic long-term stability of perovskite solar cells. Journal of Materials Chemistry A, 2020, 8(16): 7653–7658
24. Kanwat A, Choi W C, Seth S, Jang J. Doping and photon induced defect healing of hybrid perovskite thin films: an approach towards efficient light emitting diodes. ChemNanoMat: Chemistry of Nanomaterials for Energy, Biology and More, 2019, 5(5): 666–673
25. Xu Z, Liu Z, Li N, Tang G, Zheng G, Zhu C, Chen Y, Wang L, Huang Y, Li L, Zhou N, Hong J, Chen Q, Zhou H. A thermodynamically favored crystal orientation in mixed formamidinium/methylammonium perovskite for efficient solar cells. Advanced Materials, 2019, 31(24): 1900390
26. Si J, Liu Y, Wang N, Xu M, Li J, He H, Wang J, Jin Y. Green light-emitting diodes based on hybrid perovskite films with mixed cesium and methylammonium cations. Nano Research, 2017, 10(4): 1329–1335
27. Yang X, Chu Z, Meng J, Yin Z, Zhang X, Deng J, You J. Effects of organic cations on the structure and performance of quasi-two-dimensional perovskite based light-emitting diodes. Journal of Physical Chemistry Letters, 2019, 10(11): 2892–2897
28. Prakasam V, Di Giacomo F, Abbel R, Tordera D, Sessolo M, Gelinck G, Bolink H J. Efficient perovskite light-emitting diodes: Effect of composition, morphology, and transport layers. ACS Applied Materials & Interfaces, 2018, 10(48): 41586–41591
29. Naphade R, Zhao B, Richter J M, Booker E, Krishnamurthy S, Friend R H, Sadhanala A, Ogale S. High quality hybrid perovskite

semiconductor thin films with remarkably enhanced luminescence and defect suppression via quaternary alkyl ammonium salt based treatment. Advanced Materials Interfaces, 2017, 4(19): 1700562

30. Prasanna R, Gold-Parker A, Leijtens T, Conings B, Babayigit A, Boyen H G, Toney M F, McGehee M D. Band gap tuning via lattice contraction and octahedral tilting in perovskite materials for photovoltaics. Journal of the American Chemical Society, 2017, 139(32): 11117–11124
31. Xie L, Lin K, Lu J, Feng W, Song P, Yan C, Liu K, Shen L, Tian C, Wei Z. Efficient and stable low-bandgap perovskite solar cells enabled by a $CsPbBr_3$-cluster assisted bottom-up crystallization approach. Journal of the American Chemical Society, 2019, 141 (51): 20537–20546
32. Min H, Kim M, Lee S U, Kim H, Kim G, Choi K, Lee J H, Seok S I. Efficient, stable solar cells by using inherent bandgap of α-phase formamidinium lead iodide. Science, 2019, 366(6466): 749–753

Chuanzhong Yan received his B.E. degree in 2019 from College of Materials Science and Engineering, Huaqiao University, China. He is a Master's candidate in Prof. Zhanhua Wei's group at Institute of Luminescent Materials and Engineering, College of Materials Science and Engineering, Huaqiao University, China. His current research focuses on perovskite light-emitting diodes.

Kebin Lin is a Ph.D. candidate in Prof. Zhanhua Wei's group at Institute of Luminescent Materials and Engineering, College of Materials Science and Engineering, Huaqiao University, China. He received his B.E. degree in 2016 from College of Materials and Chemical Engineering, Zhongyuan University of Technology, China. His research interests include perovskite light-emitting diodes and perovskite solar cells.

Jianxun Lu is a Ph.D. candidate in Prof. Zhanhua Wei's group at Institute of Luminescent Materials and Engineering, College of Materials Science and Engineering, Huaqiao University, China. He received his B.E. degree from College of Materials Science and Engineering, Huaqiao University, China in 2017. His research interests include perovskite light-emitting diodes and perovskite solar cells.

Zhanhua Wei is a full professor at Institute of Luminescent Materials and Engineering, College of Materials Science and Engineering, Huaqiao University, China. He received his B.S. degree in 2011 from Department of Chemistry, Xiamen University, China and Ph.D. degree in 2015 from Prof. Shihe Yang's group, Department of Chemistry, The Hong Kong University of Science and Technology, China. His current research focuses on the synthesis of perovskite materials, perovskite light-emitting diodes, perovskite solar cells, and other optoelectronic devices.